数理物質科学研究科　博士論文の要約

専 攻 名　物質創成先端科学専攻
学籍番号　201130083
学生氏名　梁　文榮
学 位 名　博士（理学）
指導教員　岡田　晋

博士論文題目　First-Principles Atomistic Study of the Physical Mechanisms in the Next Generation Memory Devices (次世代メモリデバイスにおける原子レベルの物理機構に関する第一原理計算の研究)

博士論文の要約

For several decades, the semiconductor-based memory technologies such as dynamic random-access-memory (DRAM) and Flash memory have been successfully scaled down via remarkable improvements in photolithography technology, leading to large capacity, low cost, and high performance memories. However, the conventional scaling on memory devices is expected to come up against physical and technical limits in the near future. In order to overcome this problem, various new materials as the next generation memories have been proposed such as magnetoresistive RAM (MRAM) [1], ferroelectric RAM (FeRAM) [2], and phase-change RAM (PCRAM) [3], which use the properties of polarization of a ferroelectric material, magnetic tunnel junctions, and the change of resistance by phase change between crystalline and amorphous states, respectively.

Recently, a new candidate has attracted a great deal of attention as a next generation nonvolatile memory, which is resistive RAM (ReRAM) [4-10]. It uses resistive switching phenomenon of new materials, such as metal oxides [10,11] and organic compounds [12,13]. The typical ReRAM structure has a capacitor-like metal-insulator-metal (MIM) structure, where the resistive material is sandwiched by two metal electrodes as shown in Fig. 1. This simple structure enables lots of advantages such as high density, low operation power, and fast speed switching. Moreover, it has been reported that highly scalable cross-point and multilevel stacking memory structures are available, which allows larger memory capacity [14]. The resistance of insulator in the ReRAM structure is switched between the low resistance state (LRS) and the high resistance state (HRS) by applying voltage to the electrode. The switching speed between LRS and HRS is known to faster than several nanoseconds [15,16].

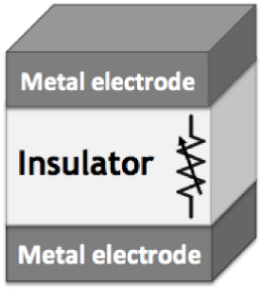

Fig. 1. Schematic illustration of ReRAM structure. ReRAM is composed of two metal electrodes and a sandwiched insulator.

The development and application of ReRAM is less advanced compared to other candidates for next

generation nonvolatile memories such as FeRAM, MRAM, and PRAM because its operation mechanism has not yet been completely understood. Therefore, investigation of a physical mechanism is a very important issue for the further development and application of ReRAM.

For the ON/OFF switching during the operation, filamentary conducting paths form as a soft breakdown at first in the dielectric material, which is called the forming process. Rupture of the filaments takes place during the reset process, and filament formation during the set process. Oxygen ions/atoms near the interface between the metal electrode and the oxide were considered as an origin of the formation and rupture of the conductive filaments [17,18]. Recently, however, it has been proposed that an oxygen vacancy (V_O) is the origin of the conductive path. For the TiO_2-based ReRAM device, Kwon, *et al*. has directly observed by high-resolution transmission electron microscopy that the filament-shape of low oxygen concentration phase, which is Magneli phase Ti_4O_7, compared to rutile or anatase phase TiO_2 [19]. Moreover, it has been reported by *ab initio* modeling that the ordering of V_Os forms the conductive channel that electrons go through in the TiO_2-based system [20]. These both experimental and theoretical results strongly suggest that V_O is an origin of the conductive filament in ReRAM.

For a physical process during the conductive path formation and disruption by applying the electric field, the drift of positively charged vacancies has been considered over the past few years [6,7,21-23]. However, the drift model is not enough to explain the nanosecond scale of switching speed of ReRAM, and it has not yet been obtained about the comprehensive understanding of the formation and disruption processes of the conductive path in ReRAM. Generally, the electronic effects, which are not considered in the drift model, in nanomaterials are crucial because the electron states strongly correlate with the atomistic structural changes, which have been observed in a variety of nanomaterials such as metal oxide nitride oxide silicon-type memory and biomolecules [24,25].

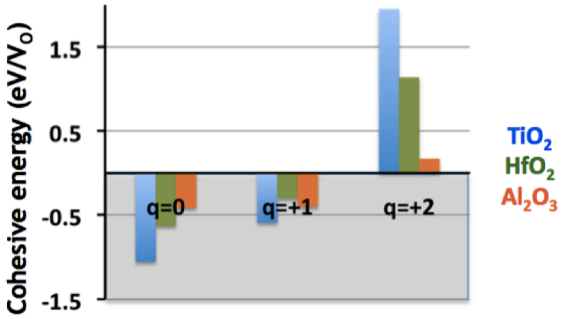

Fig. 2. Cohesive energies of TiO_2, HfO_2, and Al_2O_3. All of three oxides are likely to form V_O-filament in q=0 and q=+1 charge states [26].

In chapter 3, we performed first-principles calculations by constructing V_O models for three oxides, TiO_2, HfO_2, and Al_2O_3, in order to understand the physical mechanism of ReRAM. Fig. 2 shows cohesive energy, $E_C(q)$, per one V_O in three oxides, as a function of charge state q, by comparing the total energy between V_O-chain model and one V_O model. Based on calculation results, V_O would be isolated at q=2+, while V_O would be cohesive at q=0 and q=1+, for all three oxides. Therefore, the physical origin of the oxide-based ReRAM is the cohesion-isolation phase transition of V_O, which is

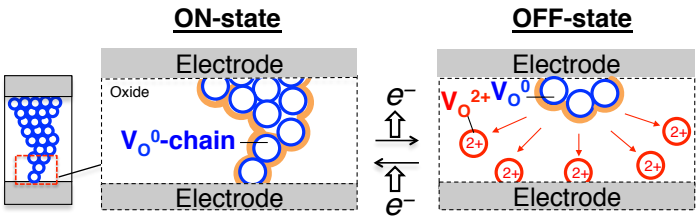

Fig. 3. Schematic illustration of ON/OFF switching in oxide-based ReRAM by electron injection/removal.

achieved by carrier injection and removal, as shown in Fig. 3.

Over a decade, the performance of ReRAM device has been drastically improved [16]. For the further improvement toward the practical use, it is required the higher performance of each memory cells, such as higher ON/OFF ratio, lower forming voltage, and lower programming current. In chapter 4, we propose the three-layer ReRAM stack structure with thin Al_2O_3 layer to obtain the high ON/OFF ratio. Al_2O_3 has the physical property that is a poor V_O former, thereby it can be used as an V_O barrier layer. Thus, V_Os are completely removed from Al_2O_3 layer at OFF-state [Fig. 4(a)], resulting in high ON/OFF ratio. On the other hand, V_Os still exists even in OFF-state in the usual ReRAM with two-layer structure [Fig. 4(b)]. Therefore, high ON/OFF ratio is obtained by introducing an Al_2O_3 V_O barrier layer. Moreover, we explain the formation mechanism of the conductive V_O filament in advanced ReRAM structure containing the thin Al_2O_3 layer in the dissertation.

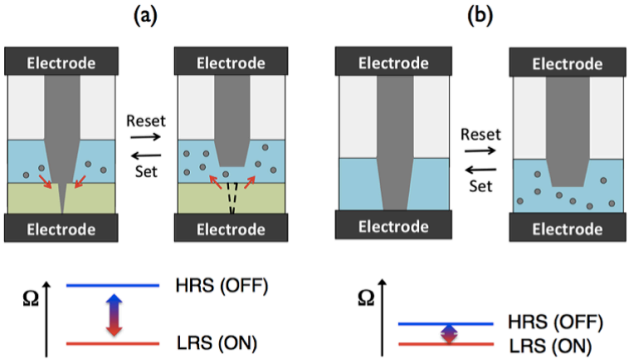

Fig. 4. Schematic illustrations of ReRAM structures (upper) and their ON/OFF ratio (down). (a) Three-layer structures involving Al_2O_3 layer as a V_O barrier layer and (b) usual two-layer structure are shown. White, sky blue, and green represent Hf, HfO_2, and Al_2O_3 layers, respectively. Gray column, gray circle, and Ω represent conductive filament, V_O, and the resistance of the system, respectively [27].

To fully understand the advanced ReRAM with the Al_2O_3 layer, the investigation of the nature of the V_O cohesion-isolation in Al_2O_3 is inevitable. In chapter 5, we discuss about the V_O diffusion mechanism in the Al_2O_3-based ReRAM in detail. By focusing on the nanoscale size of Al_2O_3 layer and the charge state of V_O, we provides not only the V_O diffusion mechanism but also a natural explanation for the discrepancy of the V_O diffusion energies between previous experimental and theoretical studies. Table I shows the calculation results of the activation energies at different charge states for all pathways. Interestingly, we observed that the activation energies depend on the charge state of V_O, which are the highest at q=0 and gradually reduced by removing the electrons from V_O for all pathways. Although the activation energy of V_O diffusion at q=2+ shows good agreement with the operation voltage on Al_2O_3-based ReRAM [29], it is much smaller than the activation energy in bulk Al_2O_3, ~5 eV [30]. Al_2O_3 has been known as a weak ionic material with covalent bond characteristic, compared to other binary oxides such as TiO_2 and HfO_2, which have been known as strong ionic bondings. Therefore, the electrons are likely to be captured in V_O site when V_O is formed [Fig. 5(a)]. The calculated activation energies of V_O diffusion at q=0

Table I. Activation energies (eV) of V_O diffusion on the four pathways at different charge states [28].

	Path 1	Path 2	Path 3	Path 4
q=0	3.90	4.70	4.33	6.01
q=1+	2.47	3.25	3.43	4.80
q=2+	1.26	1.72	2.25	3.23

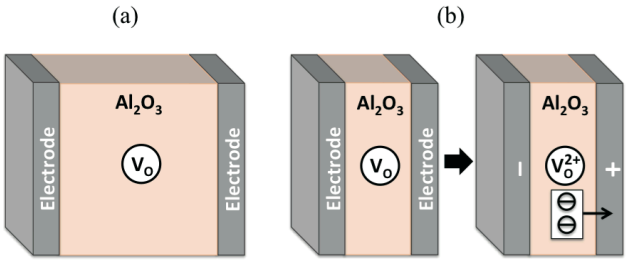

Fig. 5. Schematic illustration of V_O in the Al_2O_3 layer. (a) The charge state of V_O is difficult to be changed in bulk Al_2O_3, however (b) it can be easily changed by applying voltage in Al_2O_3 thin layer [28].

are 4~6 eV, which supports this proposal. On the other hand, the electrons can easily move to electrode by applying voltage in thin film such as ReRAM structure, the activation energy of V_O diffusion is decreased by electron removal from V_O [Fig. 5(b)]. Our results indicate that the charge state should be considered to discuss defect diffusion, especially in thin film, which provides an additional degree of freedom in nano-scale applications.

Although one of the significant advantages of ReRAM is the potential for high-density memories, it still remains many obstacles to attain further scalability such as a high voltage for a forming process and high programming currents, which make difficult to design the circuit [31-33]. Recently, it has been reported that nitrogen doping into AlO_x-based ReRAM significantly reduces the forming voltage and the programming current [34]. However, the role of nitrogen incorporation into AlO_x-based ReRAM is not fully understood, though it has been reported that nitrogen doping drastically reduces a leakage current in Hf-based metal-insulator-semiconductor field- effect-transistors (MISFETs) [35], which is likely to have a different mechanism with that in AlO_x-based ReRAM from the different electronic structures. In chapter 6, we explain the role of nitrogen incorporation into AlO_x-based ReRAM in the atomistic level. We performed calculation for four models; bulk Al_2O_3 and three different models of $Al_2O_3(V_O)$ with two N atoms. (We referred to them as Model A, Model B, and Model C, respectively.) Interestingly, we found that the formation energy of V_O in Al_2O_3 is significantly reduced by introducing N atoms [Table II]. According to Kim *et al.*, N incorporation into AlO_x-ReRAM reduced the forming voltage from ~7 eV to ~3 eV [34], which shows quite good agreement with calculated V_O formation energies. Based on above results, it is concluded that N incorporation leads to forming-free ReRAM by reducing the V_O formation energy in Al_2O_3. Moreover, N atoms that tend to couple with V_O are likely to improve the reliability of ReRAM by suppression of the V_O diffusion.

Table II. Formation energy of V_O $E(V_O)$ in bulk Al_2O_3 and Al_2O_3 with N atoms (Models A, B, and C).

	Bulk Al_2O_3	Model A	Model B	Model C
$E(V_O)$	7.96 eV	3.67 eV	3.92 eV	4.59 eV

The multilevel programming and cross-point memory structure, in which the memory cells have an area of about $4F^2$ (where F is the minimum feature size), enables to fabricate a further high-density memory. For integration of multilevel cross-point structure, the bi-directional selector is required to suppress the sneak current path. Among a various selector devices such as poly-Si, VO_2, and tunneling oxide [38-40], NbO_2 has proposed as a promising candidate for the selector device and has shown to excellent resistive switching

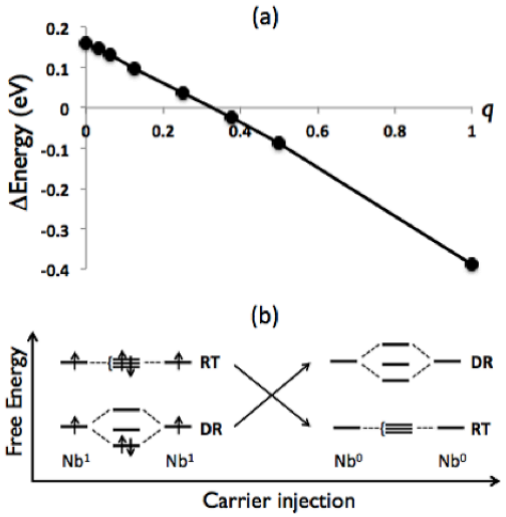

Fig. 6. (a) Energy differences (b) and schematic illustration of relative stability between rutile NbO_2 and distorted-rutile NbO_2 ($\Delta E = E_{RT} - E_{DR}$). Energy differences and charge (q) are represented per one formula unit. Arrows and bars represent electrons and energy levels, where only 4*d*-electrons are considered.

characteristics with suppressed sneak-path current [35,36]. As an origin of ON/OFF switching in oxide-based ReRAM, it has been believed to V_O as we mentioned. For the NbO_2-based selector device, however, a different mechanism should be considered because it shows the different physical properties such as an I-V characteristic. In chapter 7, we discuss a physical mechanism of resistive switching on NbO_2-based selector device, which is likely to be related to metal-insulator-transition (MIT) nature of NbO_2. NbO_2 undergoes a metal-insulator-transition (MIT) at 1081 K by structural transition from a high temperature rutile (RT) structure to a low temperature distorted-rutile (DR) structure [38,39]. To understand the resistive change by applying voltage in NbO_2, we performed first-principles calculations for both RT-NbO_2 and DR-NbO_2 structures with different charge states. Fig. 6(a) shows the energy difference between DR-NbO_2 and RT-NbO_2 as a function of the charge state. As a result, we found that the low temperature DR-NbO_2 is more stable at q=0, however RT-NbO_2 becomes stable by the electron removal. Fig. 6(b) shows schematic illustration of relative energies between RT-NbO_2 and DR-NbO_2 depending on carrier injection, where only one 4*d*-electron for a Nb atom is considered since Nb exists as an ion, Nb^{4+}, in NbO_2 crystal. At neutral charge state, the DR-NbO_2 structure is energetically stable because the degenerated states of RT-NbO_2 are splitted by distortion and the electrons occupy the more stable orbital, which is explained by Jahn-Teller effect [40]. On the other hand, the advantage by distortion disappears if the electrons are removed by applying voltage, thereby the RT-NbO_2 structure becomes energetically stable. This phase change from the low symmetric structure to the high symmetric structure, against the Jahn-Teller effect, is called anti-Jahn-Teller effect [41]. These Jahn-Teller and anti-Jahn-Teller effects clearly explain the electric field-induced MIT in NbO_2.

We have mentioned that the oxygen defect plays a crucial role in the oxide-based memory device. For the deep relationship between oxygen defects and the device performance, it has been reported to not only the ReRAM device but also for the metal-insulator-semiconductor-field-effect-transistor (MISFET). In chapter 8, we discuss about the effects of oxygen defect to MISFET. Over the past decades, the size of MISFET has continually been scaled down, which results in a chip with increased functionality in the same area. In fact, the number of transistors per a chip has been doubled in every 18 months, which is commonly referred to as Moore's law. As a result, several micrometers of MISFET channel lengths have been drastically reduced to a few tens of nanometers in modern integrated circuits [16].

The remarkable scaling down of MISFET devices has led to the notable reduction of the thickness of an insulator film, which was usually SiO_2. Thinner insulator results in higher gate leakage currents that is one of the most serious reliability issues. As a result, a high

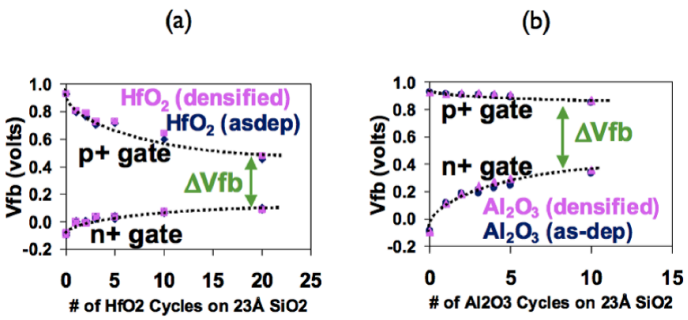

Fig. 7. Flatband voltage shifts as a function of atomic layer deposition cycles of (a) HfO_2 and (b) Al_2O_3 [42].

dielectric constant materials, which is refer to as high-*k* materials, have been proposed as alternatives to SiO_2 to avoid the large leakage current. Although Hf-based oxides had attracted much attention as the alternative to SiO_2 at first because of their promising properties such as thermal stability in contact with Si, the commercial use of Hf-based MISFET was tardy due to the Fermi level pinning that leads to difficulty in designing complimentary MOS (CMOS) circuits as shown in Fig. 7(a) [42].

In 2004, Shiraishi *et al*. proposed the oxygen vacancy model as the mechanism of Fermi level pinning to explain the V_{th} shifts observed in Hf-based MISFET [43,44]. They focused on the effect of V_O formation in HfO_2 by an interfacial reaction between HfO_2 and SiO_2. They have reported that V_O formation and subsequent electron transfer across the interface causes Fermi level pinning, especially in p+poly-Si gate MISFETs. Moreover, the proposed V_O model was extended to Hf-based MISFET with metal gate, and explained the *p*-metal Fermi level pinning as well as *p*+poly-Si pinning [45].

Similar to the Hf-based high-*k* MISFET, Fermi level pinning was also observed in Al_2O_3-based MISFET with poly-Si gate [Fig. 7(b)], which makes it difficult to use Al_2O_3 as a gate dielectrics. However, no comprehensive understanding has yet been obtained for the substantial V_{fb} shifts observed in Al_2O_3-based MISFET because V_O model is difficult to be applied to Al_2O_3-based dielectrics due to the physical property of poor V_O former [46-48]. In chapter 8, we propose the interstitial oxygen (O_i) model, instead of V_O model, to understand Fermi level pinning in Al_2O_3-based dielectrics.

By employing the precise calculation, we found that O_i defect states are located about 1 eV above the valence band top of Al_2O_3. Based on the calculation results, we schematically show the mechanism for substantial V_{fb} shifts in Al_2O_3-based dielectric [Fig. 8]. First, assuming that the SiO_2 is partially reduced, Si-O bond in SiO_2 is broken and oxygen atom moves into Al_2O_3 [Fig. 8(a)]. Fig. 8(b) shows the energy level of Al_2O_3 containing an O_i, which is located 1 eV above the valence band top of Al_2O_3. Subsequently, electrons transfer into O_i defect level of Al_2O_3 since SiO_2 is in contact with a poly-Si and the O_i level is formed under Fermi level [Fig. 8(c)]. In extremely doped case (*n*+poly-Si), large energy gain is obtained by electron transfer from the system Fermi level to the O*i* defect level in the Al_2O_3. As a result, the effective dipole is formed between Al_2O_3 and poly-Si, leading to elevation of the O_i level in Al_2O_3 [Fig. 8(d)]. It is noticeable that the energy gain in the interface reaction decreases by elevating the O*i* level position. We can infer that the position of Fermi level pinning corresponds to the energy level where the

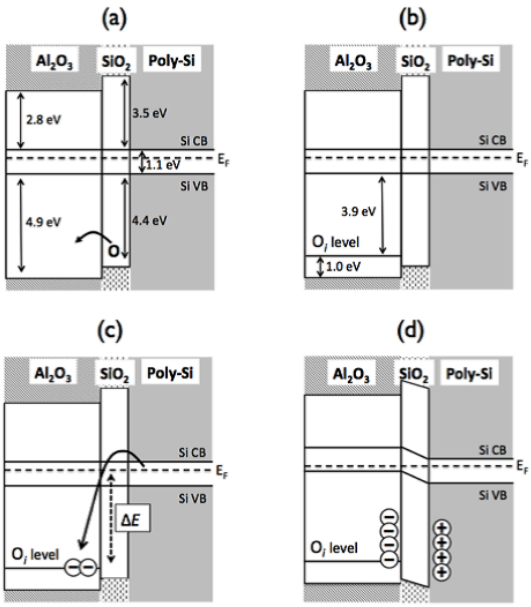

Fig. 8. Schematic illustration of O*i* formation and Fermi level pinning in Al2O3. (a) Partial reduction of SiO2 and O*i* formation in Al2O3. (b) O*i* defect level formation. (c) Electron transfer into O*i* defect level of Al2O3. (d) Accumulation of negative charges in Al2O3 and the subsequent energy level elevation [49].

energy gain of interfacial reaction becomes zero. The estimated Fermi level pinning position in the *n*+poly-Si gate is about 0.35 eV higher than the valence band top of Si, which is in quite good agreement with the experimental result [45]. In addition to V_O model in Hf-based dielectrics, O_i model is another type of defect-induced Fermi level pinning observed in Al_2O_3-based MISFET, which provides a general concept of nano-interface physics toward oxide-based applications.

Throughout this dissertation, we have proposed the physical mechanisms in the next generation memory devices, and provide guiding recipes to improve the quality of ReRAM in the atomistic level by the first-principles calculations. As an analogy phenomenon, furthermore, we have explained Fermi level pinning observed in Al_2O_3-based MISFET. We believe that our results provide an additional degree of freedom for their applications. We also hope that our results can provide a fundamental understanding of the next generation devices and be beneficial to their commercial applications.

References

[1] M. N. Babich, *et al.,* Phys. Rev. Lett. **61**, 2472 (1988). [2] J. F. Scott, *et al.,* Science **246**, 1400 (1989). [3] S. R. Ovshinsky, Phys. Rev. Lett. **21**, 1450 (1968). [4] R. Waser, *et al.*,, Nature Mater. **6**, 833 (2007). [5] A. Sawa, Mater. Today **11**, 28 (2008). [6] R. Waser, *et al.,* Adv. Mater. **21**, 2632 (2009). [7] H. Akinaga, *et al.,* Proc. IEEE **98**, 2237 (2010). [8] Y. Nishi, Current Appl. Phys. **11**, e101 (2011). [9] A. Makarov, *et al.,* Microelectron. Reliab. **52**, 628 (2012). [10] I. G. Baek, *et al.,* Tech. Dig. -Int. Electron Devices Meet. **2004**, 587. [11] W. W. Zhuang, *et al.,* Tech. Dig. -Int. Electron Devices Meet. **2002**, 193. [12] L. Ma, *et al.,* Appl. Phys. Lett. **82**, 1419 (2003). [13] R. Muller, *et al.,* Appl. Phys. Lett. **90**, 063503 (2007). [14] I. G. Baek, *et al.,* Tech. Dig. -Int. Electron Devices Meet. **2005**, 750. [15] C. Yoshida, *et al.,* Appl. Phys. Lett. **91**, 223510 (2007). [16] International Technology Roadmap for Semiconductors 2011; http://www.public.itrs.net [17] K. Kinoshita, *et al.,* Appl. Phys. Lett. **89**, 103509 (2006). [18] K. M. Kim, *et al.,* Appl. Phys. Lett. **90**, 242906 (2007). [19] D.-H. Kwon, *et al.,* Nat. Nanotechnol. **5**, 148 (2010). [20] S.-G. Park, *et al.,* IEEE Electron Device Lett. **32**, 197 (2011). [21] D. B. Strukov, *et al.,* Nature **453**, 80 (2008). [22] S. Yu, *et al.,* Tech. Dig. -Int. Electron Devices Meet. **2011**, 413. [23] D. Ielmini, IEEE Trans. Electron Devices **58**, 4309 (2011). [24] K. Yamaguchi, *et al.,* Tech. Dig. -Int. Electron Devices Meet. **2009**, 275. [25] K. Kamiya, *et al.,* Biochim. Biophys. Acta **1807**, 1328 (2011). [26] K. Kamiya, *et al.*, Tech. Dig. -Int. Electron Devices Meet. **2012**, 478. [27] M. Y. Yang, *et al.*, Jpn. J. Appl. Phys. **52**, 04CD11 (2013). [28] M. Y. Yang, *et al.*, Appl. Phys. Lett. **103**, 093504 (2013). [29] L. Goux, et al., Dig. Tech. Pap. - Symp. VLSI Technol. **2012**, 159. [30] A. H. Heuer *et al.*, Philos. Mag. Lett. **79**, 619 (1999). [31] S. Kim, *et al.*, Appl. Phys. Lett. **92**, 223508 (2008). [32] L. Chen, *et al.,* IEEE Electron Device Lett. **31**, 356 (2010). [33] Y. Wu, *et al.,* IEEE Electron Device Lett. **31**, 1449 (2010). [34] W. Kim, *et al.,* Dig. Tech. Pap. - Symp. VLSI Technol. **2011**, 22. [35] N. Umezawa, *et al.,* Appl. Phys. Lett. **86**, 143507 (2005). [36] S. Kim, *et al.,* Dig. Tech. Pap. - Symp. VLSI Technol. **2012**, 155. [37] E. Cha, *et al.,* Tech. Dig. -Int. Electron Devices Meet. **2013**, 10.4. [38] R. F. Janninck, *et al.*, J. Phys. Chem. Solids **27**, 1183 (1966). [39] T. Sakata, et al., phys. stat. sol. **20**, K155 (1967). [40] H. A. Jahn, *et al.*, Proc. R. Soc. Lond. A **161**, 220 (1937). [41] H. Kamimura, *et al.*, (Heidelberg, Springer, 2005). [42] C. Hobbs, *et al.,* Dig. Tech. Pap. - Symp. VLSI Technol. **2003**, 9. [43] K. Shiraishi, *et al.,* Jpn. J. Appl. Phys. **43**, L1413 (2004). [44] K. Shiraishi, *et al.,* Dig. Tech. Pap. - Symp. VLSI Technol. **2004**, 108. [45] Y. Akasaka, *et al.,* Jpn. J. Appl. Phys. **45**, L1289 (2006). [46] A. A. Sokol, *et al.,* Chem. Phys. Lett. **492**, 48 (2010). [47] P. Gamallo, *et al.,* Phys. Chem. Chem. Phys. **9** 5112 (2007). [48] K. Yamabe, private communication. [49] M. Y. Yang, *et al.*, AIP Advances **3**, 102113 (2013).